An Analytical Model for Deflection of Flexible Needles During Needle Insertion

Ali Asadian, Mehrdad R. Kermani, and Rajni V. Patel

Abstract— This paper presents a new needle deflection model that is an extension of prior work in our group based on the principles of beam theory. The use of a long flexible needle in percutaneous interventions necessitates accurate modeling of the generated curved trajectory when the needle interacts with soft tissue. Finding a feasible model is important in simulators with applications in training novice clinicians or in path planners used for needle guidance. Using intra-operative force measurements at the needle base, our approach relates mechanical and geometric properties of needle-tissue interaction to the net amount of deflection and estimates the needle curvature. To this end, tissue resistance is modeled by introducing virtual springs along the needle shaft, and the impact of needle-tissue friction is considered by adding a moving distributed external force to the bending equations. Cutting force is also incorporated by finding its equivalent sub-boundary conditions. Subsequently, the closed-from solution of the partial differential equations governing the planar deflection is obtained using Green's functions. To evaluate the performance of our model, experiments were carried out on artificial phantoms.

I. INTRODUCTION

Accurate minimally invasive interventions for medical diagnosis and therapeutic procedures using surgical needles is a challenging task. Flexible needles can be utilized for brachytherapy (primary application), anaesthesia, tissue/fluid sampling, ablation, neurosurgery, and deep brain stimulation particularly in regions that are difficult to access. The flexibility enables us to create curvatures along the path in order to avoid collision with obstacles or anatomical structures. Any deviation of the needle tip from its intended targeted area can reduce the effectiveness of the therapy or biopsy and cause further complications, e.g., tissue damage, under/over dosing, and misdiagnosis [1].

There is not a defined tolerance for the accuracy of tip positioning in clinical practice, but, precise placement of the tip is a difficult task due to several reasons. Needle-tissue interaction leads to tissue deformation and needle deflection. On top of that, lack of adequate sensing and maneuverability impedes finding a straightforward planning solution. Thus, surgeons may require several steering attempts in order to accurately place the needle tip. To date, researchers have explored a number of methods to improve the process of insertion and steering in soft tissue using robotic systems,

A. Asadian, M.R. Kermani, and R.V. Patel are with Canadian Surgical Technologies and Advanced Robotics (CSTAR) and the Department of Electrical and Computer Engineering, The University of Western Ontario, London, Ontario, Canada, aasadian@uwo.ca, mkermani@eng.uwo.ca, rvpatel@uwo.ca

R.V. Patel is also with the Department of Surgery, The University of Western Ontario, London, Ontario, Canada

and sophisticated modeling or image-guided techniques [1]–[6], [11]. In this respect, deformation modeling is of interest in machine vision and surgical simulation. Soft tissue is inhomogeneous and exhibits nonlinear and anisotropic behavior in general; therefore, its modeling is a common challenge for real-time applications that cannot afford significant computation time. Misra et al. [3] provided a comprehensive survey on tool-tissue interaction models in surgical simulations.

On the other hand, dynamic response analysis of beams on foundations under moving loads has been the subject of considerable research effort in transportation systems [7]. Bridges, rails and pipelines manifest important examples of beam-like structures that are designed to support moving loads. In the current work and borrowing from advanced modeling techniques utilized in vibration [8], [9], we focus on a Green's function approach and develop a deflection model that is directly linked to the interaction forces experienced by the needle during insertion. Our study is in connection with robot-assisted needle steering that is intended to guide the needle to specific targeted areas inside soft tissue.

II. PRIOR WORK

Past work has shown that deflection of flexible long needles is affected by the beveled shape of the needle tip and the mechanical properties of soft tissue. In this regard, Abolhassani and Patel [10], [11] modeled an 18-gauge needle with a beveled tip as a cantilever beam, but ignored the vertical component of friction along the insertion depth. They solved the bending-moment equation in the static regime. However, their assumption is not valid when the needle is very flexible, or stiction affects bending. Goksel et al. [12], developed two models using Finite Element Modeling (FEM) and a series of rigid bars connected by angular springs. They simulated bending of a standard prostate brachytherapy needle by hanging scaling weights at the needle tip, and identified unknown spring constants and Young's modulus. Finally, it was concluded that the angular springs model demonstrated a better accuracy and computational efficiency. One major challenge in utilizing FEM for intra-operative control is the large number of state variables which in turn contributes to an ill-conditioned control problem.

As an extensively used model, Webster et al. [13] developed an experimental kinematic model for steering a flexible beveled-tip needle in a rubber-like plastic phantom (relatively rigid tissue). According to their bicycle/unicycle model and ignoring friction and tissue deformation, the needle tip acts like a small bicycle with locked handlebars while it moves

along a fixed arc. Misra et al. [14] presented an energy-based model influenced by macroscopic and microscopic observations of needle-gel interaction. They calculated the needle deflection, and compared the energy associated with each stage of the interaction. Their results indicate that the energy of the interaction stiffness dominates the total energy. Majewicz et al. [15] experimentally investigated the effect of insertion velocity, bevel angle, and shaft diameter on curvature of the bicycle model. They statistically showed that the curvature decreased as the diameter increased. They also found no significant trend for the tip angle possibly due to the high level of viscoelasticity of the examined tissue.

Developing a bending model, needle base manipulation mechanisms could be applied to steer a flexible needle inside soft tissue [4]–[6]. Steerability is provided by asymmetric forces acting at the needle tip, but the accuracy of a model-based planning strategy relies on the validity of the employed deflection model. In this regard, a mechanics-based model similar to our proposed approach is important in practical implementations since it can be easily integrated in a feedback system for real-time control. This fact has motivated the present study as a means of developing an accurate and feasible bending model for use in intra-operative tasks.

A possible extension of the current modeling studies is to take the impact of tissue elasticity and distributed friction simultaneously into account in a dynamic fashion. The present analysis is based on the theory of beams which is accurate for slender beams whose cross sections do not undergo extreme deformation during deflection. In our study, the effect of interaction stiffness is incorporated by assuming an elastic environment across the needle shaft. Elasticity is denoted by a large number of closely-spaced translational virtual springs that act as a continuous support to the beam. Static friction mapping is also included in the deflection equations in order to develop a novel bending model.

This article is organized as follows. Section III gives details of the proposed modeling scheme. In section IV, experimental results are discussed, and conclusions and suggestions for future work are presented in section V.

III. THE PROPOSED DYNAMIC MODELING SCHEME FOR PLANAR NEEDLE DEFLECTION

In this section, an analytical method is proposed to study a cantilever beam with application in needle insertion. The simple static Euler-Bernoulli beam theory was studied in [10], [11]. In [10], the cutting force was modeled as a concentrated point load applied to the needle tip, and tissue resistance forces were assumed to cancel each other. In [11], tissue resistance force along the needle shaft was modeled as a triangularly distributed load with maximum intensity at the entry point. Using the method of superposition, the bending was then obtained. However, later on due to the use a pretty thick needle, the tissue resistance was found to be of little impact; thus, it was ignored from deflection calculations.

To describe our proposed scheme, Fig. 1 helps us to get more insight into the planar bending of a flexible needle surrounded by soft tissue. In this scheme, the compressive
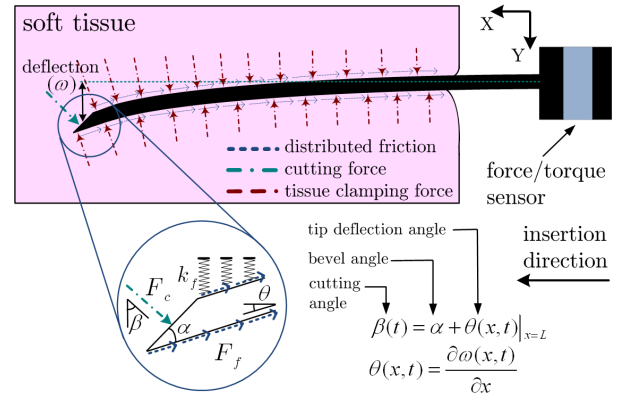

Fig. 1. Effective forces acting on the curved shaft and 2D needle deflection with respect to its insertion depth

force exerted by tissue is perpendicular to the needle shaft, and acts as a normal force that yields tangential distribution friction F_f along the tube. Unbalanced tip force F_c applied normal to the surface of the asymmetric tip is another bending factor that causes the flexible structure to deflect in the direction of the asymmetry. Thus, the needle can be considered as a partially loaded moving cantilever.

As a basis for the current analysis, let us assume that a single Euler-Bernoulli beam rests on an elastic foundation, and it is subjected to a distributed external moving load. The transversal load intensity is denoted by $f(x,t)$, and x stands for the axial distance from the base holder, the origin of our coordinate frame. The partial differential equation (PDE) governing the forced transverse motion of the neutral axis is given by [16]

$$\frac{\partial^2}{\partial x^2}\left(EI\frac{\partial^2\omega(x,t)}{\partial x^2}\right) + \rho A\frac{\partial^2\omega(x,t)}{\partial t^2} + k_f\omega(x,t) = f(x,t) \tag{1}$$

where $\omega(x,t)$ is the transversal displacement along the y direction. E and ρA are Young's modulus and the mass per unit length of the beam, respectively. I is the cross-sectional moment of inertia about the y-axis, and k_f is the load per unit length of the beam that causes the foundation to deflect by a unit amount. This parameter is a function of tissue elasticity.

Referring to Fig. 1, the needle can be split into a number of spans, and the needle curvature can be approximated by a set of linear sub-beams. Toward this goal, it is required to find an appropriate spacing of the spans, associated support types as well as the shape/direction of beam-environment contact force density functions or support stiffness values.

As depicted Fig. 1, the first span can be part of the needle that lays outside of tissue. The rest of the needle from the entry point to the tip point behaves as the second sub-beam. Thus, the needle is comprised of two uniform beams connected together at the entry point. Each sub-beam is itself an Euler-Bernoulli beam which satisfies (1). To find sub-boundary conditions, we know that the first segment is clamped at the needle holder whereas the second one has a free end, and it is subject to distributed interaction forces. On the other hand and as a result of continuity, both segments undergo the same deflection and slope, and they also experience the same amount of shear force and bending

moment at the connection point. Hence, our assumptions lead to the following sets of sub-conditions. For the first section ($0 \leq x \leq l_1$), we have

$$\omega_1(0,t) = 0, \qquad \frac{\partial \omega_1}{\partial x}(0,t) = 0$$

$$\frac{\partial^2 \omega_1}{\partial^2 x}(l_1,t) = \frac{\partial^2 \omega_2}{\partial^2 x}(l_1,t), \quad \frac{\partial^3 \omega_1}{\partial^3 x}(l_1,t) = \frac{\partial^3 \omega_2}{\partial^3 x}(l_1,t)$$

$$(2)$$

while for the second section ($l_1 \leq x \leq L = l_1 + l_2$),

$$\omega_1(l_1,t) = \omega_2(l_1,t), \qquad \frac{\partial \omega_1}{\partial x}(l_1,t) = \frac{\partial \omega_2}{\partial x}(l_1,t)$$

$$\frac{\partial^2 \omega_2}{\partial x^2}(L,t) = 0, \qquad EI\frac{\partial^3 \omega_2}{\partial x^3}(L,t) = F_c(t)cos\beta(t)$$

$$(3)$$

where the subscript i indicates the segment number, and l_i denotes the segment length. L is also the needle length, and $x = l_1$ corresponds to the skin entry point. Moreover, both sections start from rest thus ($i = 1, 2$)

$$\omega_i(x,0) = 0, \qquad \frac{\partial \omega_i}{\partial t}(x,0) = 0 \qquad (4)$$

Herein, $F_c(t)$ represents the estimated cutting force density that acts as a contact force at the tip and thereby playing as a bending factor. $\beta(t)$ is the effective angle of cutting that can be adjusted by adding the bevel angle α to the preceding instant of the tip deflection angle θ_{tip}. Initially, the needle is unbent thus $\theta_{tip}(t = 0) = \frac{\partial \omega_2}{\partial x}(L,0) = 0$.

To complete the right-hand-side of equation (1), it is worth noting that in the absence of needle-tissue interaction, for instance in the first segment, the stiffness coefficient is set to zero. The external load is also formulated as (5) where F_f is the estimated friction force density. A separate procedure has been outlined by the authors to deal with distributed dynamic friction [17]. To ease our analysis, only the vertical component of the viscous term denoted by the viscous coefficient v_f is included in the present model.

$$f(x,t) = \begin{cases} 0 & 0 \leq x < l_1 \\ F_f sin\theta(x,t) & l_1 < x \leq L \end{cases} \qquad (5)$$

For sufficiently small cutting angles, $sin\theta \approx \theta$, so this approximation simplifies the derivation of the solution to a great extent. For $\theta \leq 25^o$ that is our case, the error is at most 3% which is quite acceptable. In view of the small angle approximation, the force boundary condition at the tip expressed by (3) is revised as below.

$$EI\frac{\partial^3 \omega_2}{\partial x^3}(L,t) = F_c(t)cos\alpha - F_c(t)sin\alpha\frac{\partial \omega_2}{\partial x}(L,t) \quad (6)$$

Replacing (5) into the main PDE (1), and using the small angle approximation result in the following PDEs in which F_f is replaced by $v_f v$ where v is the insertion velocity.

$$EI\frac{\partial^4 \omega_1(x,t)}{\partial x^4} + \rho A\frac{\partial^2 \omega_1(x,t)}{\partial t^2} = 0, \quad 0 \leq x < l_1 \quad (7)$$

$$EI\frac{\partial^4 \omega_2(x,t)}{\partial x^4} + \rho A\frac{\partial^2 \omega_2(x,t)}{\partial t^2} + k_f\omega_2(x,t)$$

$$= v_f v\frac{\partial \omega_2}{\partial x}(x,t), \quad l_1 < x \leq L$$

$$(8)$$

As observed, direct inclusion of F_c and F_f into the sub-boundary conditions and the resulting PDEs incorporates the effect of interaction forces, i.e., cutting force and distributed friction, in the final solution. Knowing the value of v_f and estimating the preceding shape of the curvature, $F_c(t)$ can be directly related to the measured force in the axial direction. The term $k_f\omega(x,t)$ also takes tissue resistance into account, and models small tissue deformation in the direction of deflection. Therefore, our approach is expected to be theoretically adequate to characterize the deflection of flexible needles in soft tissue in percutaneous interventions.

Due to the geometry of our problem and having moving boundary conditions, finding the solution is not as straight-forward as standard beam-based forms extensively studied in text books [7], [16]. Applying the method of separation of variables as a common technique [16], [18] yields no time-independent modal solution for the second PDE (8); thus, this method is not applicable to our case. Instead, using a Green's function approach provides us the closed-form solution in an integral form in a computationally efficient manner [7]–[9]. In this method, the boundary conditions are embedded in Green's functions, and it is not necessary to solve the free vibration problem in order to obtain the eigenvalues and the corresponding eigenfunctions. In a truncated series solution, finding the eigenfunctions is required, and numerical convergence between two consecutive samples is not guaranteed in a moving variable-length beam.

To start, notice that a PDE with non-homogeneous boundary conditions, e.g., the second PDE (8), can always be converted to a non-homogeneous PDE with homogeneous boundary conditions [18]. The key point here is to define a transformation from the original equation to the new PDE that satisfies homogeneous boundary conditions. To this end, the desired solution for instance for the second sub-beam, namely $\omega_2(x,t)$, can be rewritten as

$$\omega_2(x,t) = \tilde{\omega}(x,t) + \phi(x,t) \qquad (9)$$

where $\phi(x,t)$ is the simplest function that satisfies the non-homogeneous boundary conditions as its counterpart, $\omega_2(x,t)$, does. For this purpose and to satisfy four existing constraints, a third-order polynomial can be chosen as below

$$\phi(x,t) = (c_3x^3 + c_2x^2 + c_1x + c_0)F_c(t) = C(x)F_c(t) \quad (10)$$

The coefficients of $C(x)$ are calculated such that $\phi(x,t)$ satisfies the non-homogeneous boundary condition implied by (6). Table I lists the coefficients obtained in this way. Considering the fact that both $\omega_2(x,t)$ and $\tilde{\omega}(x,t)$ satisfy the same boundary conditions, it is easy to show that $\tilde{\omega}(x,t)$ satisfies a set of homogeneous boundary conditions that are identical to (3) when $F_c(t)cos\alpha$ is set to 0 in (6). Thus, (8) is rewritten in terms of $\tilde{\omega}(x,t)$ as

$$EI\frac{\partial^4 \tilde{\omega}(x,t)}{\partial x^4} + \rho A\frac{\partial^2 \tilde{\omega}(x,t)}{\partial t^2} - v_f v\frac{\partial \tilde{\omega}}{\partial x}(x,t) + k_f\tilde{\omega}(x,t)$$

$$= v_f v\frac{dC(x)}{dx}F_c(t) - k_f C(x)F_c(t) - \rho A C(x)\frac{d^2 F_c(t)}{dt^2}$$

$$= \tilde{f}(x,t), \quad l_1 < x \leq L$$

$$(11)$$

2553

c_3	c_2	c_1	c_0
$\dfrac{cos\alpha}{6EI-3L^2F_c sin\alpha}$	$\dfrac{-3Lcos\alpha}{6EI-3L^2F_c sin\alpha}$	0	0

Note that the above procedure is also followed for the first segment. As obtained for $x \in [0, l_1)$, the effective force term is $-\rho A C(x)\frac{d^2 F_c(t)}{dt^2}$, but as the needle penetrates tissue, $\tilde{f}(x,t)$ comes into practice, and the governing equation for $x \in (l_1, L]$ switches to (11). $\tilde{f}(x,t)$ denotes the right-hand-side of equation (11).

Now, the dynamic Green's function method can be utilized to find the solution of the converted PDEs whose boundary conditions are homogeneous. A Green's function, named $g(x, \tilde{x}; \phi)$, is the beam response at x produced by a unit concentrated force that acts at an arbitrary position $\tilde{x}$ along the beam, and contains a single frequency component ϕ. Briefly, assuming the state variable transformation of $\tilde{\omega}(x,t) = Re\{z(x)e^{i\phi t}\}$, and taking (11) into account, z satisfies the next relationship that will give us g for $x \in (l_1, L]$. Here, δ is the Dirac delta function and $i = \sqrt{-1}$.

$$EI\frac{d^4 z}{dx^4} - v_f v\frac{dz}{dx} + (k_f - \rho A\phi^2)z = \delta(x - \tilde{x}) \quad (12)$$

To find the unknown Green's function, we employed an analogous method to what was adopted in [8] in the Laplace domain. To this end, applying Laplace transforms to (12) with respect to x, $G(s)$ for the second segment is derived as

$$G_2(s) = \frac{1}{L_2(s)} \times \left[e^{-s\tilde{x}} + (EIs^3 - v_f v)g_2(0) + EI\right.$$
$$\left.\left(s^2 g_2'(0) + sg_2''(0) + g_2'''(0)\right)\right], \quad l_1 < x \le L \quad (13)$$

where $L_2(s) = EIs^4 - v_f vs + k_f - \rho A\phi^2$, and $g_2(0)$ and its derivatives are related to the beam conditions at $x = l_1$. Similarly, for the first sub-beam, the counterpart transfer function turns out to be (14) in which $L_1(s) = EIs^4 + k_f - \rho A\phi^2$, and $g_1(0)$ and the derivatives are evaluated at $x = 0$.

$$G_1(s) = \frac{1}{L_1(s)} \times \left[e^{-s\tilde{x}} + EI\left(s^3 g_1(0) + s^2 g_1'(0)\right.\right.$$
$$\left.\left. + sg_1''(0) + g_1'''(0)\right)\right], \quad 0 \le x < l_1 \quad (14)$$

Finally, to calculate the g function over the entire beam, boundary conditions expressed earlier in this section should be transformed to the g domain [8], [9]. In general, only two out of the four initial conditions stated in (13) and (14) are explicitly known. But, equivalently we can presume that the needle is fixed, and the tissue is moving in the opposite direction. As a result, continuity conditions on g and its derivatives at $x = l_1$ as the front edge of the moving load should be satisfied [7]. This set of new constraints provide us with the missing part of the information required to find the inverse Laplace transforms of $G_1(s)$ and $G_2(s)$. Due to the complexity of the G elements, all calculations were performed using computer-aided techniques and MATLAB® symbolic toolbox.

The homogenous solution of the system can be eventually represented in terms of the convolution of the derived Green's function and the known external force [7], [9]. Finally, by adding the quasi-static solution introduced by $\phi(x,t)$ to the homogenous solution obtained using the residue theorem, the complete dynamic response of the beam can be derived. For example, for the second sub-beam

$$\omega_2(x,t) = \frac{1}{2\pi i}\int_{-\infty}^{+\infty}\left(\int_{l_1}^{L} g(x, \tilde{x}; \phi)\tilde{f}(\tilde{x},t)d\tilde{x}\right)e^{i\phi t}\, d\phi$$
$$+ C(x)F_c(t), \quad l_1 < x \le L \quad (15)$$

For more details on the mathematical method explained in brief, readers can refer to [7]–[9].

IV. IMPLEMENTATION AND EXPERIMENTS

A. Setup Description

Experimental studies of the proposed method were carried out using a state-of-the-art robotic system which has been fully designed and constructed in our lab [19]. The manipulator shown in Fig. 2 is capable of inserting, rotating, and orienting the needle with an acceptable accuracy. A Nano43 force/torque sensor (ATI Industrial Automation) with six degrees of freedom (DOF) that is attached to the needle holder and an Aurora electromagnetic tracker (Northern Digital Inc.) are the external sensing devices for providing feedback signals. Two desktop computers for control and data capturing were interfaced through a UDP connection over ethernet. The robot is controlled using a PID controller at the rate of 1kHz while force data are acquired at the rate of 100Hz after being smoothed by a moving average filter. An Aurora ultra thin 5-DOF sensor coil was also secured inside the needle shaft and very close to the tip in order to track the tip position at the rate of 40Hz. A multi-threaded application for real-time control and data communication was developed using Microsoft® C++, MATLAB® and the QuaRC® Toolbox (Quanser Inc.).

Experiments were carried out on an artificial phantom made from Gelrite Gellan Gum (Sigma-Aldrich) with two concentration rates in water: 4% (tissue A) and 6% (tissue B). This material simulates a uniform elastic environment, and mimics the frictional effects of biological tissues better than rubber phantoms. For the tests, the cannula of an 22-gauge stainless steel needle of length L=203mm was used. Imaging the needle tip by a trinocular microscope (Madell Technology Corp.), the bevel angle was estimated on the image as α=24.8°. The needle also had outer and inner diameters of 0.718mm and 0.413mm, respectively.

B. Experimental Results

The aim of the experiments was to validate the model proposed in section III. For this purpose, the estimated curve was compared with the measured deflection using the electromagnetic tracker. Furthermore, to investigate the effect of velocity, insertion through each phantom was performed at two different velocities which were far from the stiction.
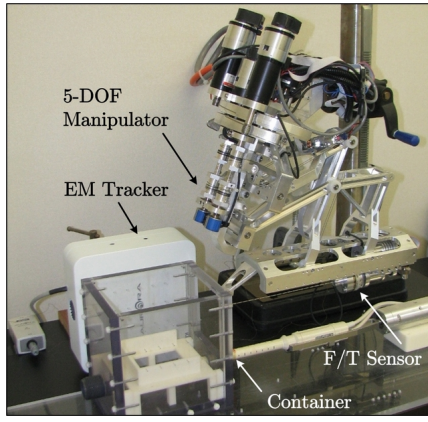
Fig. 2. A view of our robotic system for needle insertion

Fig. 3. Deflection versus insertion depth: (a) v=10mm/s, tissue A; (b) v=10mm/s, tissue B; (c) v=15mm/s, tissue A; (d) v=15mm/s, tissue B

Using a simple compression test [20], k_f was measured from the force-deformation mapping of samples of the examined phantoms with known geometries. Based on this, k_f was therefore set to 3.87kN/m^2 for tissue A and 7.65kN/m^2 for tissue B. Furthermore, the values of v_f for phantoms A and B were respectively set to 123.9Ns/m^2 and 166.7Ns/m^2 using a cone-tip version of the needle [17]. Other numerical parameters were selected as follows: ρ=8000Kg/m^3, A=2.709×10^{-7}m^2, E=200GPa, and I=1.162×10^{-14}m^4.

The needle tip was initially placed in contact with the phantom so that $l_1 = L - vt$. Generating a constant-velocity trajectory, it was discretized into a series of steps, and numerical integration using Gaussian quadrature rule was calculated over the length of the sub-beams at each step. Running the pivoting algorithm resulted in 9.3mm as the average distance between the tip and the coil center [21]. The position of the coil center is the actual reference point for comparison so the bending was evaluated at x_{coil}=L-9.3mm. In the conducted experiments, the maximum insertion forces for tissues A and B were measured to be 0.232N and 0.276N respectively at v=15mm/s. It was also observed that during the very first portion of insertion, the deflection curve did not follow the beam model. This discrepancy can be justified by the presence of rupture as an unmodelled phenomenon so it was taken into account when analyzing the results.

Fig. 3 demonstrates the empirical and the estimated deflection curve at x_{coil} for an 80mm insertion, and Table II summarizes the numerical results obtained. In the plotted graphs, the origin has been assumed to be located at the tissue entry point. As seen in Fig. 3, our method in general exhibits acceptable performance. Taking estimation error into account, the first interpretation at this point is that the model slightly outperforms for tissue B. For tissue A, as shown in Figs. 3(a) and 3(c), there exists a gradually increasing error with increasing depth. Despite this, the maximum error that occurred at the tip area in Fig. 3(a) was confined to 0.374mm which is acceptable. As another result, we conclude that inserting the needle with a higher velocity or in a phantom with a lower stiffness results in a smaller radius of curvature, and thereby providing greater needle steerability. The stiffness effect agrees with the simulation results reported in [14].
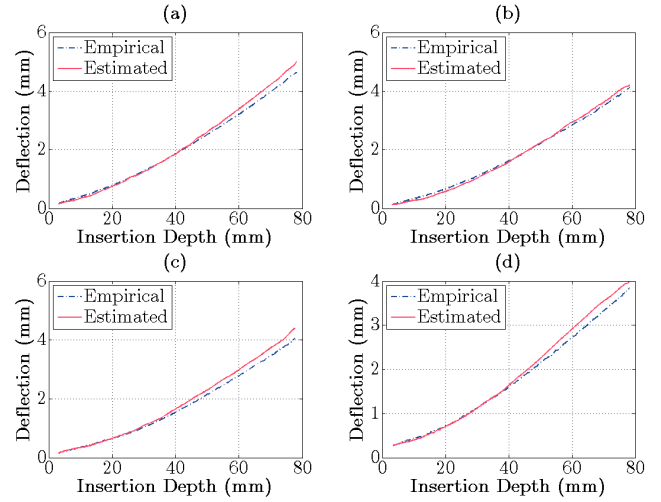
TABLE II
NUMERICAL RESULTS OF DEFLECTION ESTIMATION

	v=10mm/s		v=15mm/s	
	tissue A	tissue B	tissue A	tissue B
Average of absolute error (mm)	0.108	0.091	0.121	0.094
Maximum of absolute error (mm)	0.374	0.201	0.351	0.236
Measured radius of curvature (mm)	1357.6	1495.9	1247.8	1441.5
Estimated radius of curvature (mm)	1165.5	1292.7	1139.2	1171.7

Assuming a fixed radius of curvature throughout the entire intervention corresponds to the bicycle model introduced in [13], and later on widely exploited for control [4], [5], [10]. Thus, it is an important benchmark for comparison. We utilized a least-squares method to fit a circle to each curve in order to determine the radius of curvature. Referring to Table II, this parameter was underestimated by our model in the four studied cases, and its percentage error varied from 8.7% (case c) to 18.72% (case d). The percentage error is defined as the absolute prediction error divided by the measured value. Note that variation of each curvature during intervention can be related to the complex behavior of soft tissue, and entails a comprehensive biomechanical investigation. It is visible in the last 20mm and 10mm of the insertion depths in Figs. 3(b) and 3(d), respectively.

In the next test, robustness in the presence of uncertainty was assessed. The parameters k_f and v_f are the two that are most likely to be erroneous. In other words, finding or estimating their values requires further modeling simplification. Thus, it is worth finding out how the model performs when it encounters parametric uncertainty. The outcome imposes a limit on our confidence in the model response.

For this study, a ±20% deviation from the nominal values was introduced in both k_f and v_f, and the deviation of the estimated radius of curvature was calculated. The results are listed in Table III. To highlight the main trends, we can say that the model was more robust to overestimation of the value of k_f rather than to underestimation of this parameter since there was less change in the amount of percentage error. In

TABLE III

PERCENTAGE ERROR IN THE RADIUS OF CURVATURE IN THE
PRESENCE OF PARAMETRIC UNCERTAINTY

	v=10mm/s		v=15mm/s	
	tissue A	tissue B	tissue A	tissue B
$\Delta k_f = +20\% k_f$	12.29	8.60	9.01	11.58
$\Delta k_f = -20\% k_f$	24.61	19.22	12.75	27.84
$\Delta v_f = +20\% v_f$	15.07	14.39	12.51	21.76
$\Delta v_f = -20\% v_f$	13.80	8.85	8.97	16.53

addition, the model was less sensitive to the overestimation of v_f compared with the underestimation of k_f at the examined velocities. They both have the same impact on the estimated curvature. As indicated, a 20% stiffness increase or a 20% viscosity decrease could improve the estimation performance by almost 5% for tissue B at 10mm/s. Note that due to the experimental limitation in terms of lack of versatile phantom types needed to expose a wide range of friction properties and elasticity, no general conclusion can be inferred here.

Overall, the acceptable results presented in this work proves the capability of our model to deal with needle-tissue interaction causing the needle to flex. Part of the existing discrepancy can possibly be attributed to the simplified force diagram depicted in Fig. 1. For example, we presumed that (1) the cutting force has a single concentrated component at the tip face; (2) the needle-tissue interaction can be described by linear elasticity with a constant parameter k_f. However, the cutting mechanism in practice is not yet well formulated, and the interaction is influenced by complex factors, e.g., tissue inhomogeneity and viscoelasticity. On top of that, inaccurate approximation of interaction-related parameters such as k_f and v_f can lead to more deviation from reality.

V. CONCLUSION AND FUTURE WORK

Flexible needles can be employed in clinical practice. They have a great potential to improve targeting accuracy. Work is in progress to develop robotic systems that can accomplish needle-based interventions. Finding an accurate model is the first step toward precise control thus the deflection model will be part of the control design. In our past bending studies [10], [11], friction as a major component present in needle-tissue interaction has been disregarded, notwithstanding that its impact on bending could be considerable in some applications. In this study, friction along the insertion depth as well as the mechanical properties of the elastic medium and insertion velocity were integrated into the Euler-Bernoulli beam element. The geometry of the studied problem led to a set of PDEs for two sub-beams with coupled non-homogeneous moving boundary conditions. Green's functions were utilized as a sophisticated means to find the sought analytical solution. Theoretical results were validated using experiments, and the experimental results confirmed that the suggested technique could open up new possibilities for deflection modeling.

For the sake of simplicity, the uniform elastic foundation was assumed to be linear in our discussion. However, nonlinear viscoelasticity and nonhomogeneity will be studied in the future to represent a more realistic behavior of needle-tissue interaction. It will enable us to extend the proposed model to biological tissues, and predict the needle path during

clinical interventions. Thorough robustness test and statistical analysis are subjects of ongoing research. Investigating the impact of dynamic friction [17] is also left for future studies. Ultimately, our analytical approach which is a feasible solution is aimed at robot-assisted needle steering to improve targeting accuracy in percutaneous therapies and biopsies.

VI. ACKNOWLEDGMENTS

REFERENCES

[1] N. Abolhassani, R. Patel, and M. Moallem, Needle Insertion into Soft Tissue: A Survey, *Med. Eng. Phys.*, vol. 29, 2007, pp. 413-431.
[2] S.P. DiMaio, S.E. Salcudean, Needle Insertion Modeling and Simulation, *IEEE Trans. Robot. Autom.*, vol. 19, no. 5, 2003, pp. 864-875.
[3] S. Misra, K.T. Ramesh, and A.M. Okamura, Modeling of Tool-Tissue Interactions for Computer-Based Surgical Simulation: A Literature Review, *Presence-Teleop. Virt.*, vol. 17, no. 5, 2008, pp. 463-491.
[4] R. Alterovitz, A. Lim, K. Goldberg, G.S. Chirikjian, and A.M. Okamura, "Steering Flexible Needles under Markov Motion Uncertainty," *In Proc. of IEEE/RSJ Int. Conf. on Intel. Rob. Sys. (IROS)*, Canada, 2005, pp. 120-125.
[5] A. Asadian, M.R. Kermani, and R.V. Patel, Robot-Assisted Needle Steering Using a Control Theoretic Approach, *J. Intell. Robot. Syst.*, vol. 62, no. 3-4, pp. 397-418, 2011.
[6] V. Duindam, J. Xu, R. Alterovitz, S. Sastry, and K. Goldberg, Three-Dimensional Motion Planning Algorithms for Steerable Needles Using Inverse Kinematics, *Int. J. Rob. Res.*, vol. 29, 2010, pp. 789-800.
[7] L. Fryba, *Vibration of Solids and Structures Under Moving Loads*, Thomas Telford Ltd.; 1997.
[8] M. Abu-Hilal, Forced Vibration of Euler-Bernoulli Beams by Means of Dynamic Green Functions, *J. Journal Sound Vibrat.*, vol. 267, 2003, pp. 191-207.
[9] S.Y. Lee, H.Y. Ke, and Y.H. Kuo, Analysis of Non-Uniform Beam Vibration, *J. Journal Sound Vibrat.*, vol. 142(1), 1990, pp. 15-29.
[10] N. Abolhassani, R.V. Patel, and F. Ayazi, Minimization of Needle Deflection in Robot-Assisted Percutaneous Therapy, *Int. J. Med. Robotics Comput. Assist. Surg.*, vol. 3, 2007, pp. 140-148.
[11] N. Abdolhassani, R.V. Patel, "Deflection of a Flexible Needle During Insertion into Soft Tissue," *In Proc. of 28th IEEE EMBS Annu. Int. Conf.*, USA, 2006, pp. 3858-3861.
[12] O. Goksel, E. Dehghan, and S.E. Salcudean, Modeling and Simulation of Flexible Needles, *Med. Eng. Phys.*, vol. 31, 2009, pp. 1069-1078.
[13] R.J. Webster III, J.S. Kim, N.J. Cowan, G.S. Chirikjian, and A.M. Okamura, Nonholonomic Modeling of Needle Steering, *Int. J. Rob. Res.*, vol. 25, no. 5/6, 2006, pp. 509-525.
[14] S. Misra, K.B. Reed, B.W. Schafer, K.T. Ramesh, and A.M. Okamura, "Observations and Models for Needle-Tissue Interactions," *In Proc. of IEEE Int. Conf. on Rob. Autom. (ICRA)*, Japan, 2009, pp. 2687-292.
[15] A. Majewicz, T.R. Wedlick, K.B. Reed, and A.M. Okamura, "Evaluation of Robotic Needle Steering in *ex vivo* Tissue," *In Proc. of IEEE Int. Conf. on Rob. Autom. (ICRA)*, USA, 2010, pp. 2068-2073.
[16] S.S. Rao, *Vibration of Continuous Systems*, John Wiley and Sons Inc.; 2007.
[17] A. Asadian, R.V. Patel, and M.R. Kermani, "A Distributed Model for Needle-Tissue Friction in Percutaneous Interventions," *In Proc. of IEEE Int. Conf. on Rob. Autom. (ICRA)*, China, 2011, pp. 1896-1901.
[18] R. Haberman, *Elementary Applied Partial Differential Equation with Fourier Series and Boundary Value Problems*, Prentice Hall; 1987.
[19] H.S. Bassan, R.V. Patel, and M. Moallem, A Novel Manipulator for Percutaneous Needle Insertion: Design and Experimentation, *IEEE/ASME Trans. Mechatron.*, vol. 14, no. 6, 2009, pp. 746-761.
[20] K.A. Ross, M.G. Scanlon, Analysis of the Elastic Modulus of Agar Gel by Indentation, *J. Texture Stud.*, vol. 30, no. 1, 1999, pp. 17-27.
[21] http://www.ndigital.com/medical/aurora.php